J|A|C|S
ARTICLES

Published on Web 12/16/2009

Activation of Molecular Oxygen by a Dioxygenase Pathway by a Ruthenium Bis-bipyridine Compound with a Proximal Selenium Site

Alexander Laskavy,[†] Linda J. W. Shimon,[‡] Leonid Konstantinovski,[‡] Mark A. Iron,[‡] and Ronny Neumann*,[†]

Department of Organic Chemistry and Chemical Research Support Unit, Weizmann Institute of Science, Rehovot, Israel 76100

Received June 9, 2009; E-mail: Ronny.Neumann@weizmann.ac.il

Abstract: A ruthenium(II) bipyridine complex with proximal phenylselenium tethers, **[Ru](H$_2$O)$_2$**, reacted *intramolecularly* with O_2 in a protic slightly acidic solvent, 1,1,1,3,3,3-hexafluoro-2-propanol (HFIP), to yield an O−O bond cleaved product, **[Ru](O)$_2$**, with formation of two Ru−O−Se moieties. This stable compound was isolated, and its structure was determined by X-ray diffraction. The identification of the compound in solution was confirmed by ESI-MS and the ^{1}H NMR with the associated Curie plot that showed that **[Ru](O)$_2$** was paramagnetic. The magnetic susceptibility was 2.8 μ_B by Evan's method suggesting a ground state triplet or biradical. DFT calculations, however, predicted a ground state singlet and an oxidized Se atom. Further it was shown that **[Ru](O)$_2$** is a potent oxygen transfer species of both O_2-derived atoms to triphenylphosphine and a nucleophilic alkene such as 2,3-dimethyl-2-butene in both HFIP and acetonitrile. UV−vis spectroscopy combined with the measured stoichiometry of PPh_3:O_2 = ∼2 in a catalytic oxidation of PPh_3 suggests a dioxygenase type activation of O_2 with structural identification of the O−O bond cleavage reaction step, formation of **[Ru](O)$_2$** as an intermediate, and the proof that **[Ru](O)$_2$** is a donor of both oxygen atoms.

1. Introduction

The activation of molecular oxygen is of fundamental importance and presents an important, difficult, scientific challenge in the context of oxidation catalysis that also may have consequences in the area of "green chemistry".[1] The chemistry of ground state O_2 is mechanistically complicated.[2] Thus, O_2 ubiquitously reacts with hydrocarbons by a free radical auotoxidation mechanism. The initial hydroperoxide is typically unstable under reaction conditions, and often nonselective product formation is observed.[3] Some metal complexes can mediate electron transfer or oxidase type oxidation of organic substrates with or without concomitant oxygen transfer where O_2 is used to reoxidize the catalyst.[4,5] The activation of O_2 in the "biological world" for hydrocarbon (alkane, alkene) oxidation is attained through use of monooxygenase type enzymes where reducing agents and protons (*coreactants*) supply the energy for the cleavage of the O−O bond that leads to formation of water and reactive high-valent metal species such as iron-oxo species.[6]

The literature shows that there are only a few synthetic catalytic systems that use O_2 only, i.e. without a coreagent, for hydrocarbon oxidation. (i) Notable is the *gas phase* process for ethene epoxidation and related epoxidations of substrates without allylic hydrogen atoms.[7] (ii) The formation of OsO_4 and its use for *syn* alkene dihydroxylation was described.[8] (iii) Sterically hindered ruthenium porphyrins were shown to catalyze alkene epoxidation,[9] and a similar mechanism has been postulated by us for O_2 activation with ruthenium substituted polyoxometalates.[10] (iv) In related research, an iron(IV)-oxo species that oxidized triphenylphosphine has been reported to be formed by

[†] Department of Organic Chemistry.
[‡] Chemical Research Support Unit.

(1) (a) Punniyamurty, T.; Velusamy, S.; Iqbal, J. *Chem. Rev.* **2005**, *105*, 2329. (b) Mallat, T.; Baiker, A. *Chem. Rev.* **2004**, *104*, 3037.
(2) (a) *Modern Oxidation Methods*; Backvall, J. E., Ed.; Wiley-VCH: Weinheim, Germany, 2004. (b) Simandi, L. I. *Advances in Catalytic Activation of Dioxygen by Metal Complexes*; Kluwer Academic: Boston, USA, 2003. (c) Sawyer, D. T. *Oxygen Chemistry*; Oxford University Press: New York, 1991.
(3) (a) Walling, C. *Struct. Energ. React. Chem. Ser.* **1995**, *2*, 24–65. (b) Partenheimer, W. *Catal. Today* **1995**, *23*, 69. (c) Mayo, F. R. *Acc. Chem. Res.* **1968**, *1*, 193. (d) Hermans, I.; Peeters, J.; Jacobs, P. A. *Top. Catal.* **2008**, *50*, 124.
(4) (a) Stahl, S. S. *Angew. Chem., Int. Ed.* **2004**, *43*, 3400. (b) Feringa, B. L. In *Transition Metals for Organic Chemistry Volume 2*; Beller, M., Bolm, C., Eds.; Wiley-VCH: 1998; p 307.
(5) (a) Neumann, R. *Prog. Inorg. Chem.* **1998**, *47*, 317. (b) Kozhevnikov, I. V. *Catalysts for Fine Chemical Synthesis, Volume 2*; Catalysis by Polyoxometalates; Wiley: Weinheim, Germany, 2002.
(6) (a) *Cytochrome P-450*, 2nd ed.; Ortiz de Montellano, P., Ed.; Marcel Dekker: New York, 1995. (b) Sono, M.; Roach, M. P.; Coulter, E. D.; Dawson, J. H. *Chem. Rev.* **1996**, *96*, 2841. (c) Costas, M.; Mehn, M. P.; Jensen, R.; Que, L., Jr. *Chem. Rev.* **2004**, *104*, 939. (d) Tshuva, E. Y.; Lippard, S. J. *Chem. Rev.* **2004**, *104*, 987. (e) Que, L., Jr.; Tolman, W. B. *Angew. Chem., Int. Ed.* **2002**, *41*, 1114. (f) Solomon, E. I.; Brunold, T. C.; Davis, M. I.; Kemsley, J. N.; Lee, S. K.; Lehnert, N.; Neese, F.; Skulan, A. J.; Yang, Y. S.; Zhou, J. *Chem. Rev.* **2000**, *100*, 235.
(7) (a) Kilty, P. A.; Sachtler, W. M. H. *Catal. Rev.* **1974**, *10*, 1. (b) Barteau, M. A. *Top. Catal.* **2003**, *22*, 3. (c) Monnier, J. R.; Peters, K. T.; Hartley, G. W. *J. Catal.* **2004**, *225*, 374.
(8) (a) Döbler, C.; Mehltretter, G.; Beller, M. *Angew. Chem., Int. Ed.* **1999**, *38*, 3026. (b) Döbler, C.; Mehltretter, G.; Sundermeier, U.; Beller, M. *J. Am. Chem. Soc.* **2000**, *122*, 10289. (c) Döbler, C.; Mehltretter, G.; Sundermeier, U.; Beller, M. *J. Organomet. Chem.* **2001**, *621*, 70–76.

Scheme 1. O_2 Activation on Ruthenium−Selenium Complexes

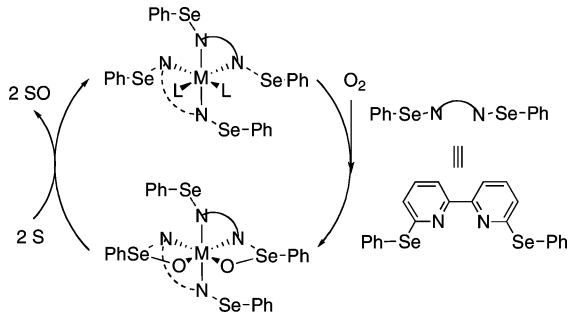

addition of O_2 to an iron(II)-cyclam complex.[11] In both the ruthenium and iron catalyzed systems,[9–11] the mechanisms for formation of the reactive metal-oxo intermediates and the O−O bond cleavage step have not been structurally established although the O_2 activation step was followed by spectroscopy.

Herein we describe a dioxygenase type catalyst for O_2 activation that enables cleavage of the O−O bond and the observation of the O−O bond cleavage via isolation of the reactive metal-oxo intermediate. To this end we have prepared 2,2-bipyridine ligands with arylselenium tethers. The concept for O_2 activation and subsequent oxygen transfer is presented in Scheme 1.

This compound was designed as such because of (a) its α-*cis* conformation, (b) the proximity of the adjacent oxophilic selenium, (c) the significant steric hindrance around the transition metal center, and (d) the possibility for intramolecular O_2 activation. The α-*cis* conformation is advantageous because it can enable the binding of O_2 at the metal center and lead, after cleavage of the oxygen−oxygen bond, to a *cis*-dioxo species that are known as effective oxygen donors. The proximal selenium center is favorable for first aiding in the cleavage of the oxygen−oxygen bond by introduction of an oxophilic element and second for stabilization of the metal-oxo intermediate formed. The steric hindrance around the transition metal center is important to avoid formation of intermolecular μ-peroxo species that often disproportionate to μ-oxo species that are "dead-end" thermodynamically stable compounds. The intramolecular O_2 activation is advantageous relative to the previously reported intermolecular O_2 activation because it will allow heterogenization of the catalyst in the future, which will be important for epoxidation of important gaseous substrates such as propene.

2. Results and Discussion

The 6,6′-bis-phenylselenyl-2,2′-bipyridine ligand was prepared by the CsOH catalyzed alkylation[12] of 6,6′-dibromo-2,2′-bipyridine with diphenydiselenide. The Ru(II) compound was then prepared along the lines of a literature preparation[13] to yield the required Ru(II) compound with arylselenium tethers and two labile L = H_2O or CH_3CN ligands [Ru(6,6′-$(SePh)_2$-2,2′-bipy$)_2$(L$)_2$](X$)_2$ (**[Ru](L)$_2$**), L = H_2O or CH_3CN; X = counteranion. The X-ray structure of **[Ru](ACN)$_2$** indeed shows the expected slightly distorted octahedral complex with an α-*cis* conformation, Figure 1 and Table 1. The six Ru−N distances are 2.033, 2.042, 2.075, 2.080, 2.080, and 2.108 Å. The distances between the Ru and Se atoms are in the range of 3.593 to 3.628 Å respectively; there are no bonding interactions between the Ru and Se atoms.

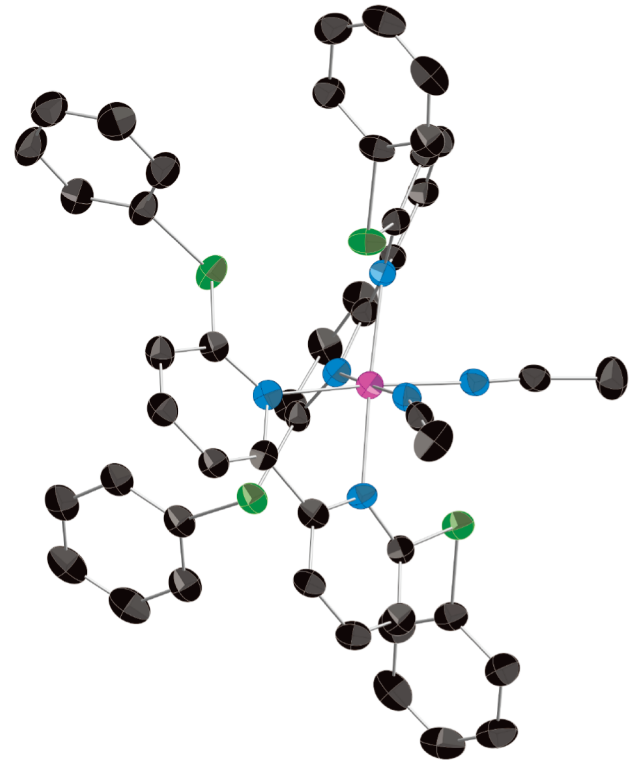

Figure 1. ORTEP drawing (50% probability) of **[Ru](ACN)$_2$** (Ru, magenta; Se, green; N, blue; C, black; solvent molecules, counteranions, and hydrogen atoms are not shown for clarity).

Table 1. Key Interatomic Distances and Angles for **[Ru](ACN)$_2$**

Bond Lengths, Å		Bond Angles, deg			
Ru1 N1	2.080(5)	N1 Ru1 N6	177.2(2)	N2 Ru1 N4	103.9(2)
Ru1 N2	2.108(5)	N4 Ru1 N5	171.8(2)	N2 Ru1 N6	100.6(2)
Ru1 N3	2.075(5)	N1 Ru1 N4	97.4(2)	N2 Ru1 N5	80.2(2)
Ru1 N4	2.080(5)	N4 Ru1 N6	85.4(2)	N3 Ru1 N1	101.2(2)
Ru1 N5	2.033(6)	N6 Ru1 N5	86.9(2)	N3 Ru1 N4	79.0(2)
Ru1 N6	2.042(5)	N5 Ru1 N1	90.4(2)	N3 Ru1 N5	96.9(2)
		N2 Ru1 N3	177.1(2)	N3 Ru1 N6	79.4(2)
		N2 Ru1 N1	78.7(2)		

The analogous aqua complex **[Ru](H$_2$O)$_2$**, was extensively characterized by HR-ESI-MS; IR; and ^{1}H, ^{13}C, ^{15}N, and ^{77}Se NMR spectroscopy (see Figures S5−S11). The ESI-MS showed the expected molecular ion cluster (without anions) of peaks at m/z = 1069 and a cluster of peaks at m/z = 517 assignable to [M − (2 × H_2O)]/2. The ^{1}H, ^{13}C, ^{15}N, and ^{77}Se NMR spectra all showed that the compound is nonsymmetric. For example, four peaks were observed in the ^{15}N NMR for the N atoms of bipy at δ = 237.21, 249.89, 253.11, and 256.72 ppm. Similarly, four peaks were observed in the ^{77}Se NMR at δ = 491.42, 493.40, 501.69, and 502.15 ppm.

The Ru(II) compound **[Ru](H$_2$O)$_2$** was dissolved in 1,1,1,3,3,3-hexafluoro-*iso*-propanol (HFIP) and reacted with O_2 at RT for 48 h. It should be noted that such a slightly acidic solvent was

(9) (a) Groves, J. T.; Quinn, R. *J. Am. Chem. Soc.* **1985**, *107*, 5790. (b) Groves, J. T.; Ahn, K. H. *Inorg. Chem.* **1987**, *26*, 3831. (c) James, B. R.; Pacheco, A.; Rettig, S. J.; Thorburn, I. S.; Ball, R. G.; Ibers, J. A. *J. Mol. Catal.* **1987**, *41*, 147.
(10) (a) Neumann, R.; Dahan, M. *Nature* **1997**, *388*, 353. (b) Neumann, R.; Dahan, M. *J. Am. Chem. Soc.* **1998**, *120*, 11969.
(11) Kim, S. O.; Sastri, C. V.; Seo, M. S.; Kim, J.; Nam, W. *J. Am. Chem. Soc.* **2005**, *127*, 4178.
(12) Varala, R.; Ramu, E.; Adapa, S. R. *Bull. Chem. Soc. Jpn.* **2006**, *79*, 140.
(13) Collin, J. P.; Sauvage, J. P. *Inorg. Chem.* **1986**, *25*, 135.

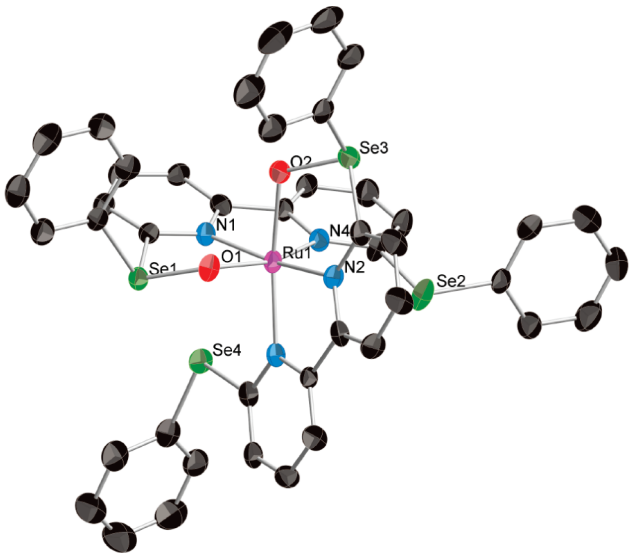

Figure 2. ORTEP drawing (50% probability) of **[Ru](O)$_2$** (Ru, magenta; Se, green; N, blue; O, red; C, black; solvent molecules, counteranions, and hydrogen atoms are not shown for clarity).

Table 2. Key Bond Lengths and Angles for **[Ru](O)$_2$**

Bond Lengths, Å			
Ru1 N1	2.000(6)	Ru1 O1	2.093(5)
Ru1 N2	2.004(6)	Ru1 O2	2.096(6)
Ru1 N3	2.099(7)	Se1 O1	1.733(5)
Ru1 N4	2.080(7)	Se3 O2	1.723(6)
Bond Angles, deg			
Equatorial Plane		Axial Plane	
O2 Ru1 N3	164.2(2)	N1 Ru1 N2	168.2(3)
O1 Ru1 N4	164.6(2)	N1 Ru1 N4	79.7(3)
O1 Ru1 O2	85.8(2)	N2 Ru1 N4	107.2(3)
N2 Ru1 N3	79.1(3)	N1 Ru1 O1	86.0(2)
N4 Ru1 N3	102.1(2)	N2 Ru1 O1	86.1(2)
O1 Ru1 N3	87.8(2)	N1 Ru1 O2	84.8(2)
Ruthenium-Oxygen-Selenium		N2 Ru1 O2	86.0(2)
Se3 O2 Ru1	110.4(3)	N1 Ru1 N3	109.2(3)
Se1 O1 Ru1	111.3(3)	N2 Ru1 N3	79.1(3)

needed for this reaction; acetonitrile gave no product. From this reaction we were able to isolate and crystallize the intended **[Ru](O)$_2$** compound whose X-ray diffraction derived structure is shown in Figure 2. Important bond lengths and angles are listed in Table 2. The structure shows the presence of two oxygen atoms between the ruthenium and selenium sites. The Se−O bond lengths (1.723−1.733 Å) are longer than that observed for SeO (1.634 Å)[14] but very similar to the bond length for SeO^- (1.726 Å)[15] as may be expected for a bridging situation. The Ru−O bond lengths of ∼2.09 Å are also longer than those expected for a terminal Ru−O bond (1.5−1.8 Å). The Ru−O−Se bond angles are slightly larger than the

(14) Verma, K. K.; Reddy, S. P. *J. Mol. Spectrosc.* **1977**, *67*, 360.
(15) Coe, J. V.; Snodgrass, J. T.; Freidhoff, C. B.; McHugh, K. M.; Bowen, K. H. *J. Chem. Phys.* **1986**, *84*, 618.

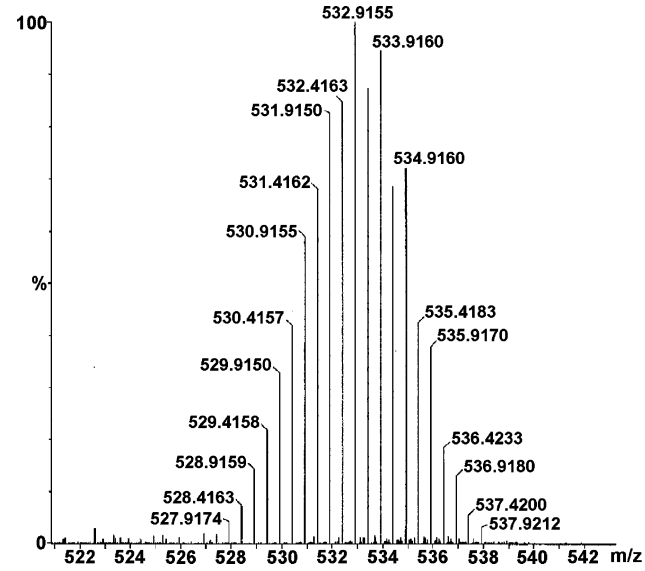

Figure 3. High resolution ESI MS of **[Ru](O)$_2$**.

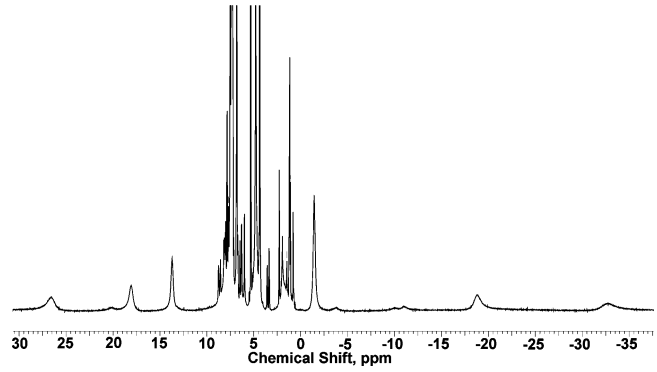

Figure 4. ^{1}H NMR of **[Ru](O)$_2$** at 216 K.

tetrahedral angle. Therefore, the Ru−O and Se−O bond lengths and the Ru−O−Se bond angles are consistent with an oxygen atom bound to and bridging between the Ru and Se atoms. The O−O distance is 2.851 Å clearly indicating that the O_2 molecule has been cleaved.[16]

The high resolution positive ion mode ESI-mass spectra, Figure 3, of **[Ru](O)$_2$** shows the expected cluster of peaks at $m/z = 533$ which is attributable to the half mass of the molecular peaks (without anion and solvent). The ^{1}H NMR of **[Ru](O)$_2$** taken at 216 K clearly shows that **[Ru](O)$_2$** is paramagnetic with peaks appearing at chemical shifts ranging from −32.8 to 26.6 ppm, Figure 4. Plots of the ^{1}H NMR spectra as a function of temperature and then plots of the chemical shifts as a function of temperature (Figures S12−13) show a linear behavior consistent with a Curie paramagnetic species. Not surprisingly **[Ru](O)$_2$** was EPR silent down to 120 K because, as the NMR suggests, the relaxation times are very fast. Also, measurement of the magnetic moment by the Evan's method yielded $\mu_{eff} = 2.8\ \mu_B$ which is roughly consistent with two unpaired spins.

(16) Sterically hindered Ru^{II}(2,9-dimethyl-1,10-phenanthroline)$_2$(H_2O)$_2$ has been reported (UV−vis spectra only) to yield dioxo species upon reaction with H_2O_2. In HFIP the reaction of Ru^{II}(2,9-dimethyl-1,10-phenanthroline)$_2$(H_2O)$_2$ with O_2 showed no change in the UV−vis spectrum and no formation of Ru-oxo compounds. (a) Goldstein, A. S.; Beer, R. H.; Drago, R. S. *J. Am. Chem. Soc.* **1994**, *116*, 2424. (b) Goldstein, A. S.; Drago, R. S. *J. Chem. Soc., Chem. Commun.* **1991**, 21.

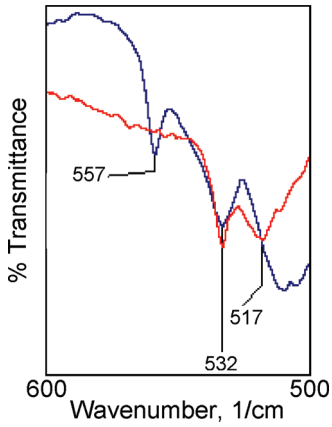

Figure 5. Region where differences were observed in the IR spectra of **[Ru]**(^{16}**O**)$_2$ (blue) and **[Ru]**(^{18}**O**)$_2$ (red).

Table 3. Selected Bond Distances (Å) in **[Ru](O)$_2$** (Atomic Labels Refer to the Calculated Structures Depicted in *Figure S15*)

	[Ru]O$_2$		
Bond	Singlet	Triplet	X-ray
O(81)−O(82)	2.837	3.223	2.851
O(81)−Se(84)	1.739	1.755	1.733
O(82)−Se(86)	1.739	1.731	1.723
O(82)−Ru(83)	2.134	2.215	2.095
O(81)−Ru(83)	2.134	2.078	2.092
N(77)−Ru(83)[a]	2.020	2.137	2.004
N(78)−Ru(83)[b]	2.108	2.177	1.999
N(79)−Ru(83)[a]	2.020	2.010	2.040
N(80)−Ru(83)[b]	2.108	2.376	2.099
Se(84)−C(42)	1.965	1.954	1.950
Se(84)−C(53)	1.928	1.929	1.926
Se(86)−C(46)	1.964	1.983	1.942
Se(86)−C(65)	1.928	1.936	1.910

[a] Mutually *trans* pyridine rings. [b] Pyridine ring *trans* to O.

The ^{1}H NMR spectra and magnetic susceptibility measurements clearly suggest that **[Ru](O)$_2$** is not diamagnetic.

The IR spectra of **[Ru](H$_2$O)$_2$** and **[Ru](O)$_2$** were also compared (Figure S14). Most interesting in this context is the IR assignment of the Ru−O−Se moiety that was identified by comparison of the IR spectra of **[Ru](O)$_2$** and **[Ru](**^{18}**O)$_2$**, the later being prepared from **[Ru](H$_2$O)$_2$** and $^{18}O_2$. Thus the peaks at 557 and 517 cm^{-1} can be assigned to the Ru−O−Se and Ru−^{18}O−Se vibrations, respectively, Figure 5. The isotopically shifted peak in the IR spectrum at 517 cm^{-1} is close to the expected absorption at 525 cm^{-1}.

Considering that for the starting complex, **[Ru](H$_2$O)$_2$**, the oxidation states of the Ru and Se sites are both formally 2+, a four electron oxidation with O_2 indicates the possibility of three most likely electronic configurations for **[Ru](O)$_2$**: (i) $Se^{II}\cdots O-Ru^{VI}-O\cdots Se^{II}$, (ii) $Se^{IV}-O^{-}\cdots Ru^{II}\cdots {}^{-}O-Se^{IV}$, or (iii) $Se^{III}-O-Ru^{IV}-O-Se^{III}$. Since both ruthenium and selenium invariably take on low spin configurations, a working hypothesis based on the experimental evidence for the assignment of the oxidation states in **[Ru](O)$_2$** is that the compound has a low spin Ru^{IV} and two Se^{III} centers. The calculated (DFT) structure of **[Ru](O)$_2$** is depicted in Figure S15 that includes also the atomic numbering scheme used for the calculated structure. Selected bond lengths for both the singlet and triplet states along with their corresponding experimental X-ray crystallography measured equivalents are listed in Table 3. In this context, it should be noted that there is reasonable agreement between the calculated and measured geometries for a ground state singlet and a poorer agreement for a triplet state. Likewise, there is reasonable agreement in the analogous bond distances in **[Ru](ACN)$_2$** (see Table S1).

Table 4. Selected Natural Bond Orbital Results for **[Ru](O)$_2$**

		Ru(83)	Se(84)	Se(85)
NPA	Core	35.987	27.997	27.998
	Valence	7.313	4.472	5.523
	Rydberg	0.101	0.052	0.033
	Total	43.402	32.520	33.554
	Charge	0.598	1.480	0.446
Natural Electron Configuration		[core] $4d^{7.05}5s^{0.26}$	[core]$4s^{1.64}4p^{2.83}$	[core]$4s^{1.72}4p^{3.81}$

The measured singlet−triplet gap at the M06/SDB-cc-pVDZ//M06-L/SDB-cc-pVDZ/DBFS level of theory is 1.05 eV. (For comparison, at the M06-L/SDB-cc-pVDZ/DBFS level, the gap is 1.07 eV.) To check whether M06 has a tendency to over- or underestimate this gap, the vertical singlet−triplet gap (i.e., the difference between the singlet and triplet energies calculated for the singlet geometry) was calculated for a number of different exchange-correlation functionals such as B3LYP, PBE, and PBE0, Table S2. All the functionals predict a lower energy for the singlet state. Accounting for differences in zero-point vibrational energies (ZPVE) at the M06-L/SDB-cc-pVDZ/DBFS level also led to a lower energy singlet state. It should, however, be noted that these calculations are at 0 K while the measurements were carried out above 200 K.

An additional question that was probed by the DFT calculations is with regards to the formal oxidation states of the selenium and ruthenium atoms in **[Ru](O)$_2$**. The NBO analysis shows that significant positive charge is localized on the selenium atoms. Table 4 shows the natural population analysis for Se84 (bound to O, similar results are obtained for Se86), Se85 (not bound to O, similar results are obtained for Se87), and Ru83. On comparison of the two selenium atoms, it was observed that there is clearly less electron density on Se84/Se86 than on Se85/Se87. Note that there is no real physical meaning to the absolute value of charge calculated. One can note that the results obtained in **[Ru](O)$_2$** for Se85 (not bound to O) are very similar to those obtained for the selenium atoms in **[Ru](ACN)$_2$**, Table S3, where these atoms are undisputedly Se^{II}. Thus, if one accepts that Se85/Se87 is Se^{II}, as it is bound to two aryl rings, then Se84/Se86 would formally have a higher oxidation state, e.g. Se^{III} or Se^{IV}.

Although the experimental results indicate a triplet state for **[Ru](O)$_2$** from which we hypothesize low spin Ru^{IV} and two Se^{III} centers, that is $Se^{III}-O-Ru^{IV}-O-Se^{III}$, the DFT calculations indicate a singlet ground state with a more likely $Se^{IV}-O^{-}\cdots Ru^{II}\cdots {}^{-}O-Se^{IV}$ configuration. Relevant to this dichotomy is also the observation that, as will be shown below, **[Ru](O)$_2$** is an oxygen donor. This typically implies a higher valent ruthenium-oxo active species.

The UV−vis spectra of **[Ru](H$_2$O)$_2$** and **[Ru](O)$_2$** are very similar and relatively featureless. We were, however, interested in the evolution of the O_2 cleaved species that was more easily observable by measurement of difference UV−vis spectra, Figure 6. The difference spectra showed an isosbestic point at 297 nm indicating a clean bimolecular transformation of **[Ru](H$_2$O)$_2$** plus O_2 to **[Ru](O)$_2$** on the measured time scale.

The reactivity of **[Ru](O)$_2$** was tested under a variety of conditions. First, in stoichiometric reactions 3 μmol of **[Ru](O)$_2$** were reacted with 30 μmol of PPh_3 in 1.5 mL of HFIP under Ar. After 2 h at RT a 19.7% conversion (5.9 μmol) of PPh_3 to

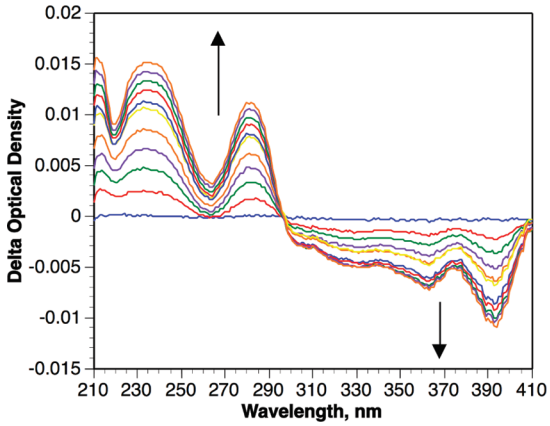

Figure 6. Difference spectra showing the evolution of **[Ru](O)$_2$** from 1.8 μM **[Ru](H$_2$O)$_2$** at 25 °C in HFIP blanketed by 1 bar of O_2. Spectra measured every 15 min.

PPh_3=O was measured by GC proving nearly complete oxygen transfer of *both* O atoms. Although as noted above **[Ru](O)$_2$** is not formed in acetonitrile, it can be isolated and then reacted in this solvent. For example, 3 μmol of **[Ru](O)$_2$** was reacted with 30 μmol of PPh_3 in 1.5 mL of acetonitrile under Ar. After 8 h at RT a 19.3% conversion (5.8 μmol) of PPh_3 to PPh_3=O was measured by GC proving nearly complete, albeit slower, oxygen transfer of *both* O atoms. This reactivity was verified by (a) reaction of PPh_3 with ^{18}O labeled **[Ru](^{18}O)$_2$** yielding PPh_3=^{18}O (>95% ^{18}O labeled) and (b) measurement of the ESI-MS of the reaction mixture with time that showed the disappearance of **[Ru](O)$_2$** (m/z = 533) concomitant with the appearance of **[Ru](O)(H$_2$O)** (m/z = 525) and then **[Ru](H$_2$O)$_2$** (m/z = 517). At the end of the reaction mostly **[Ru](H$_2$O)$_2$** was observed along with a small amount of **[Ru](O)(H$_2$O)**. Similarly, **[Ru](O)$_2$** is reactive toward a nucleophilic alkene such a 2,3-dimethyl-2-butene in both HFIP and acetonitrile. Thus, 7.4 μmol of **[Ru](O)$_2$** and 42 μmol of 2,3-dimethyl-2-butene were reacted in 1.5 mL of solvent at 23 °C, under Ar. In acetonitrile, the reaction yielded, after 12 h, 15.3 μmol (96%) of 2,3-dimethyl-2-butene oxide. In HFIP, the reaction yielded, after 4 h, 15.1 μmol (94%) of 3,3-dimethyl-2-butanone (pinacolone) and traces of 2,3-dimethyl-2,3-butanediol (pinacol). Apparently the acidity of the HFIP solvent leads to the hydrolysis of the initial epoxide formed and its subsequent pinacol rearrangement to the final product. This was verified by reacting 2,3-dimethyl-2-butene oxide in HFIP. Second, a catalytic oxidation of PPh_3 with O_2 catalyzed by **[Ru](H$_2$O)$_2$** (600 μmol of PPh_3, 30 μmol of **[Ru](H$_2$O)$_2$**, 8.8 mL of HFIP, 26 °C under 1 bar of O_2 in a gas buret) showed a PPh_3:O_2 stoichiometry of 1.98 indicating that a dioxygenase pathway to PPh_3=O indeed is operating. The turnover frequency was 0.83 h^{-1}.

Given the results collected and presented above, one may present a working hypothesis for the activation of O_2 by **[Ru](H$_2$O)$_2$**, Scheme 2. The reaction is initiated by coordination of O_2 to **[Ru](H$_2$O)$_2$** via ligand exchange. In a likely proton assisted step, a protonated Ru(III)-superoxo species undergoes rearrangement enabled by the proximal Se sites to yield the stable **[Ru](O)$_2$** compound, which in the presence of a reactive substrate is a viable oxygen transfer species. Two lines of evidence support in general terms such a dioxygenase activation of O_2. First, the observation of the formation of **[Ru](O)$_2$** from **[Ru](H$_2$O)$_2$** by UV−vis spectroscopy appears to indicate a clean one-step transformation. Second, the catalytic oxidation of PPh_3 with O_2 catalyzed by **[Ru](H$_2$O)$_2$** showed a requisite PPh_3:O_2 stoichiometry of ∼2. A third desired line of evidence would be to react **[Ru](H$_2$O)$_2$** with a 1:1 mixture of $^{16}O_2$:$^{18}O_2$ and analyze the **[Ru](^{16}O)$_2$:[Ru](^{18}O)$_2$** ratio by ESI-MS; no **[Ru]^{16}O^{18}O** should be formed. Unfortunately, this experiment failed because the activated O atom is freely exchanged by water present in the electrospray ionization source used to analyze **[Ru](^{18}O)$_2$**. Additional and numerous attempts to use other MS methods, such as MALDI-TOF-MS with various matrices and Field Desorption-MS, did not give molecular peaks, but rather fragmentation products (both methods) and substitution of the oxygen atom by the matrix (MALDI-TOF).

One should emphasize that the data available to date do not exclude the possibility of a bimolecular mechanism for the activation of O_2, for example via a **[Ru]O$_2$[Ru]** intermediate. Considering, however, the steric bulk around the ruthenium metal center, we are suggesting an intramolecular O_2 activation mechanism as an initial working hypothesis.

3. Conclusions

Synthesis of an octahedral ruthenium(II) compound based on a 2,2′-bipyridyl ligand with proximal arylselenium tethers at the 6,6′ position led to a compound, **[Ru](H$_2$O)$_2$**, with two labile aqua ligands at the α-*cis* positions. Crystals for solid state identification, Figure 1, were available by preparation of the analogous **[Ru](ACN)$_2$**. Reaction of **[Ru](H$_2$O)$_2$** with O_2 showed by UV−vis, Figure 6, a one-step transformation to a ruthenium dioxo species, **[Ru](O)$_2$**, that was identified in the solid state by X-ray crystallography, Figure 2, and showed the formation of two Ru−O−Se moieties that were also identified by IR spectroscopy, Figure 5. In solution, HR-ESI-MS, Figure 3, showed the requisite m/z (z = 2) cluster of molecular peaks. The ^1H NMR, Figure 4, and the associated Curie plots showed that **[Ru](O)$_2$** is paramagnetic. The magnetic susceptibility by Evans' method was 2.8 μ_B. This value is close to a triplet or biradical and suggests a formulation of oxidation states in **[Ru](O)$_2$** as Se^{III}−O−Ru^{IV}−O−Se^{III}. An alternative formulation is suggested by DFT calculations at 0 K which pointed toward a ground state singlet and oxidized Se atoms, more likely a Se^{IV}−O^-···Ru^{II}···$^-$O−Se^{IV} formulation. The dichotomy between the experimental evidence and the calculated results remains unresolved; however, it should be stressed that **[Ru](O)$_2$** is a potent oxygen donor, capable of transferring both oxygen atoms originally derived from O_2 as demonstrated by formation of **[Ru](^{18}O)$_2$** from **[Ru](H$_2$O)$_2$** and $^{18}O_2$. The fact that **[Ru](O)$_2$** was indeed reactive toward nucleophiles such as triphenylphosphine and 2,3-dimethyl-2-butene suggests that the ruthenium center is indeed partly in a higher oxidation state, since it would

Scheme 2. Proposed Mechanism for Formation of **[Ru](O)$_2$**

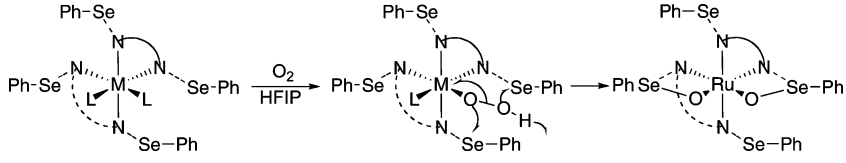

appear more likely based on literature precedence[3,9] that a higher valent Ru-oxo species would be an oxygen donor versus a $Se^{IV}-O^{-}\cdots Ru^{II}\cdots{}^{-}O-Se^{IV}$ configuration which would perhaps be expected to be inert as an oxygen donor. Future research will be devoted to more reactive analogues of **[Ru](H$_2$O)$_2$** that will be able to activate O_2 and oxygenate less nucleophilic terminal aliphatic alkenes.

4. Experimental Section

4.1. Synthetic Procedures. 6,6′-Bis-phenylselenyl-2,2′-bipyridine (**bipySePh**). 1.51 g (4.8 mmol) of 6,6′-dibromo-2,2′-bipyridine, 2.25 g (7.2 mmol) of diphenyl diselenide ($(SePh)_2$), and 2.19 g (13.1 mmol) of $CsOH\cdot H_2O$ in 14.4 mL of dry DMSO were stirred under Ar at 110 °C for 6 h. The DMSO was distilled off under vacuum, and the remaining solid was washed 5 times with H_2O. The ligand was purified on a silica gel column using 65/35 CH_2Cl_2/*n*-hexane as eluent. Yield = 67.1% (3.13 g) (white microcrystalline product). Elemental Analysis, calculated: C, 56.67%; H, 3.46%; N, 6.01%. Found: C, 56.49%; H, 3.39%; N, 5.96%. For further characterization, see Supporting Information, Figures S1−S4.

[Ru(6,6′-$(SePh)_2$-2,2′-bipy)$_2$$(H_2O)_2$]$(PF_6)_2$ (**[Ru](H$_2$O)$_2$**). 105 mg (0.40 mmol) of $RuCl_3\cdot xH_2O$, 424 mg (0.91 mmol) of **bipySePh**, and 268 mg (6.32 mmol) of LiCl were stirred in 2.6 mL of ethylene glycol under Ar at 150 °C for 10 h. The mixture was cooled to RT, and the preciptate formed was washed with H_2O until the wash was colorless and then dried under vacuum overnight. The precipitate was dissolved in 40 mL of MeOH, and 300 mL of Et_2O were slowly added while stirring to yield a brown microcrystalline precipitate. The wash with Et_2O was continued until all the free ligand was extracted and nearly pure Ru(6,6′-$(SePh)_2$-2,2′-bipy)$_2$$Cl_2$ was obtained (ESI-MS: *m*/*z* - 1104.70). Yield = 77.4% (324 mg). Ru(6,6′-$(SePh)_2$-2,2′-bipy)$_2$$Cl_2$ (324 mg) was dissolved in 2.0 mL of acetonitrile (ACN) under Ar, and 17 mL of H_2O were added and the solution was heated at 60 °C for 3 h. The reaction mixture was cooled to 0−5 °C. Five drops of HPF_6 (65% in water) and 702 mg of NH_4PF_6 in 8.8 mL of H_2O were added. After 2 h the brown microcrystalline precipitate was collected and washed 4 times with 100 mL of 0.1 M HPF_6 and dried under vacuum overnight. Yield = 97.6% (388 mg) (brown microcrystalline product). Elemental Analysis, calculated: C, 41.99%; H, 2.88%; N, 4.45%. Found: C, 41.59%; H, 2.76%; N, 4.57%. For further characterization, see Supporting Information, Figures S5−S11.

[Ru(6,6′-$(SePh)_2$-2,2′-bipy)$_2$$(ACN)_2$]$(ClO_4)_2\cdot NaClO_4$ (**[Ru](ACN)$_2$**) for X-ray structure determination was similarly prepared. Thus, 50 mg (0.045 mmol) of Ru(6,6′-$(SePh)_2$-2,2′-bipy)$_2$$Cl_2$ in 0.3 mL of ACN under Ar were treated with 5.0 mL of H_2O at 60 °C for 3 h. After cooling to 0−5 °C, 1.5 mL of a saturated solution of $NaClO_4$ in 0.1 M $HClO_4$ was added dropwise. After 2 h, the brown microcrystalline precipitate was washed 5 times with 15 mL of 0.1 M aq. $HClO_4$ and dried under vacuum. Yield = 91.4% (46 mg). Orange-brown prismatic crystals were grown from a solution in ACN by slow addition of benzene vapors. Elemental Analysis, calculated: C, 40.12%; H, 2.67%; N, 5.85. Found: C, 39.87%; H, 2.58%; N, 5.67%.

[Ru(6,6′-$(SePh)_2$-2,2′-bipy)$_2$$(O)_2$]$(PF_6)Cl\cdot x CHCl_3$ (**[Ru](O)$_2$**). 9.5 mg (8.9 μmol) **[Ru](H$_2$O)$_2$** were dissolved in 2.0 mL of HFIP in a 20 mL glass tube and placed under 1 bar of O_2 and stirred for 48 h at RT. After evaporation of the solvent and drying under vacuum, the remaining solid was dissolved in 2.0 mL of $CHCl_3$. Black needle-like crystals were grown by slow addition of *n*-hexane vapors. Yield 88% (10.6 mg). Elemental Analysis, calculated: C, 32.18%; H, 2.04%; N, 3.07%. Found: C, 32.55%; H, 2.08%; N, 2.91%. For further characterization, see Figures 3−5 and S12−14.

4.2. Characterization. 4.2.1. X-ray Structure Determination. For **[Ru](ACN)$_2$**: Crystal data were collected at 120 K using a Nonius Kappa CCD diffractometer with Mo Kα (λ = 0.710 73 Å) radiation. The data were processed with Denzo-scalepack. The structures were solved by direct methods with SHELXS. Full-matrix least-squares refinement was based on F^2 with SHELX-97. 33 181 (9972 unique) reflections (R_{int} = 0.078) were collected over a range of q = 2.55−25.68 with $-15 \le h \le 14$, $-17 \le k \le 17$, $0 \le l \le 20$. $2\theta_{max}$ = 51.36°, from a crystal of size of 0.15 × 0.15 × 0.15 mm^3; the largest electron density peak 1.841 eÅ^{-3} and hole −1.108 dÅ^{-3}. For **[Ru](O)$_2$**: Crystal data collected at 100 K using a Bruker Kappa ApexII CCD diffractometer with Mo Kα (λ = 0.710 73 Å) radiation and Miracol optics. The data were processed with the Bruker Apex2 suite, and the structure was solved with direct methods in Bruker Apex2 Autostructure. Full-matrix least-squares refinement was based on F^2 with SHELX-97. 97 880 (12 593 unique) reflections (R_{int}= 0.071) were collected over a range of q = 2.63−25.68 with $-26 \le h \le 26$, $-26 \le k \le 25$, $-25 \le l \le 26$. $2\theta_{max}$ = 51.36°, from a crystal of size 0.20 × 0.05 × 0.05 mm^3; largest electron density peak 2.876 eÅ^{-3} and hole −1.570 eÅ^{-3}.

Table 5. Crystal Data and Structure Refinement for Compounds **[Ru](ACN)$_2$** and **[Ru](O)$_2$**

Compound	[Ru](ACN)$_2$	[Ru](O)$_2$
Empirical formula	$C_{48}H_{38}N_6RuSe_4$ + Na+3ClO_4	$C_{44}H_{32}N_4O_2RuSe_4$+ PF_6 + Cl + 29/6$CHCl_3$
Formula weight	1437.09	1823.01
Space group	Triclinic, $P\bar{1}$	Rhombohedral, $R\bar{3}$
a, Å	12.830(3)	21.8438(4)
b, Å	14.283(3)	21.8438(4)
c, Å	16.894(5)	21.8438(4)
α, deg	90.61(2)	99.34(1)
β, deg	104.71(2)	99.34(1)
γ, deg	116.42(1)	99.34(1)
V (Å^3), Z	2654.2(13), 2	9956.3(3), 1
d_{calc} (mg/cm^3)	1.798	1.824
μ (mm^{-1})	3.264	3.136
R [$I > 2\sigma(I)$][a]	R_1 = 0.0580, wR_2 = 0.1430	R_1 = 0.0591 wR_2 = 0.1525
R (all data)	R_1 = 0.0877; wR_2 = 0.1542	R_1 = 0.1121; wR_2 = 0.1984

[a] $R_1 = \Sigma||F_0| - |F_c||/\Sigma$; $wR_2 = \{\Sigma[w(F_0^2 - F_c^2)^2]/\Sigma w(F_0^2)^2]\}^{1/2}$.

4.2.2. NMR Spectroscopy. ^{1}H, ^{13}C{^{1}H}, ^{15}N, and ^{77}Se{^{1}H} NMR spectra were recorded at 298 or 216 K as noted (in $CDCl_3$ or CD_2Cl_2) on a 500 MHz spectrometer operating at 500.13, 125.76, 50.70, and 95.38 MHz respectively, using 5 mm sample tubes. The ^{1}H and ^{13}C chemical shifts were referenced to TMS; ^{15}N chemical shifts were referenced to liquid NH_3. ^{77}Se chemical shifts are relative to Me_2Se (external standard selenophene, δ = 605 ppm).[17] The pulse programs of the gsCOSY, ^{13}C−^{1}H gsHMQC, and ^{15}N−^{1}H gsHMBC experiments were used from the Bruker software library. The gradient HMBC was acquired using SW = 90 ppm with 256 increments in F1 and 96 transients per increment. Long-range coupling was 7 Hz.

4.2.3. Mass Spectrometry. Low resolution spectra were taken on an MS Micromass ZMD 4000 Mass Spectrometer equipped with an ESI probe for electrospray analysis. High resolution spectra were taken on a UPLC-MS Micromass Q-TOF Premier spectrometer equipped with ESI for electrospray analysis.

4.2.4. IR Spectroscopy. The FT-IR spectra were measured on a Nicolet 6700 FTIR; samples were prepared by evaporation of samples of **[Ru](H$_2$O)$_2$**, **[Ru]((^{16}O)$_2$**, and **[Ru]((^{18}O)$_2$** on KBr plates.

4.2.5. UV−vis Spectroscopy. UV−visible spectra were recorded on an Agilent 89090A spectrophotometer using the following experimental procedure: A 1.8 μM solution of **[Ru](H$_2$O)$_2$** was prepared by dissolving 0.573 mg (0.540 μmol) of [Ru(6,6′-$(SePh)_2$-2,2′-bpy)$_2$ $(H_2O)_2$]$(PF_6)_2$ in 100 μL of $CHCl_3$ (cleaned from peroxides by neutral alumina and degassed by He, and then blanketed by Ar). Then 1 μL of this solution was added to 3.0 mL of $CF_3-CH(OH)-CF_3$ (degassed by He and placed under Ar). To

(17) Choi, M.-G.; Angelici, R. J. *J. Am. Chem. Soc.* **1991**, *113*, 5651.

observe the formation of **[Ru](O)$_2$** a quartz cuvette was placed under 1 bar of O_2 at 25 °C.

4.2.6. Elemental Analyses. Elemental analyses (C, H, N) were performed on a CHN elemental analyzer (FlashEA 1112, Eager 300 Software).

4.3. Oxygen Transfer Reactions. The reaction between **[Ru](O)$_2$** and Ph_3P or 2,3-dimethy-2-butene was carried out in HFIP or acetonitrile under Ar in a 25 mL pressure tube using the amounts given in the paper. The products and substrates were quantified using a GLC with a flame ionization detector and a 30 m × 0.32 mm 5% phenylmethylsilicone (0.25 μm coating) capillary column and helium carrier gas. Products identified by GC-MS. A catalytic reaction to determine the PPh_3:O_2 stoichiometry was carried out in a 25 mL flask attached to a oxygen buret. Conditions: 600 μmol of PPh_3, 30 μmol of **[Ru](H$_2$O)$_2$**, 8.8 mL of HFIP, 26 °C under 1 bar of O_2.

4.4. Computational Methods. Calculations are at the PCM-(CH_3CN)-M06/SDB-cc-pVDZ//M06-L/SDB-cc-pVDZ/BFBS level of theory. All calculations were carried out using Gaussian 03 Revision E.01[18] to which the MNGFM patch[19] was applied; this patch from the University of Minnesota adds the M06 (*vide infra*) family of DFT exchange-correlation functionals to the commercial version. Two DFT exchange-correlation functionals were used. The first is the new M06 functional,[20] a meta-hybrid functional containing 27% HF exchange, which was shown to have even superior performance in the study of transition metal reactions. The second is the local version of the M06 family (M06-L).[21] This functional was shown to provide similar performance as M06 for transitional metals.[20] With this functional, the SDB-cc-pVDZ combines the Dunning cc-pVDZ basis set[22] on the main group elements and the Stuttgart-Dresden basis set-RECP[23] on the transition metals with an added *f*-type polarization exponent taken as the geometric average of the two *f*-exponents given in the appendix of ref 24. The cc-pVDZ-PP basis set-RECP combination of Peterson et al. was used on selenium.[25]

Density Fitting Basis Sets (DFBS), as implemented in Gaussian03,[26] were employed to improve the computational efficiency of the calculation. Because of the large size of the ligands (87 atoms, 450 electrons), the use of DFBSs is essential to be able to optimize the geometries in a reasonable amount of time. Because the use of DFBSs precludes the use of a hybrid DFT exchange-correlation functional, the local version of the M06 family (M06-L) was employed.[21] This functional was shown to provide performance similar to that M06 for transitional metals.[20] Truhlar recently recommended its use in such a scheme for optimizing large complexes followed by energy calculations with either M06 or M06-2X as appropriate (the former in this case because of the presence of a transition metal).[27] The automatic DFBS generation algorithm built-in to Gaussian03 was employed.

The geometries of **[Ru]O$_2$** were fully optimized as both a singlet and a triplet. Bulk solvent effects were approximated by single-point energy calculations using a polarizable continuum model (PCM),[28] specifically the integral equation formalism model (IEF-PCM)[28] with water as the solvent as in the experiments. Explicit spheres were used on the hydrogen atoms.

For interpretive purposes, natural population analysis (NPA) charges[29] were derived from natural bond order (NBO) analyses calculated at the M06/SDB-pc1//M06-L/SDD(d)/DFBS level of theory. Mulliken charges[30] are also provided, although the NPA charges are generally considered to be more reliable.

Acknowledgment. The research was supported by the German-Israeli Project Cooperation (DIP-G7.1), the Israel Science Foundation, the Helen and Martin Kimmel Center for Molecular Design, and the Bernice and Peter Cohn Catalysis Research Fund. R.N. is the Rebecca and Israel Sieff Professor of Organic Chemistry.

Supporting Information Available: X-ray cif files and NMR, IR, and mass spectra. This material is available free of charge via the Internet at http://pubs.acs.org.

JA9047027

(18) Frisch, M. J. *Gaussian 03*, revision E.01; Gaussian, Inc.: Wallingford, CT, 2004.
(19) Minnesota Gaussian Functional Module version 3.1; Zhao, Y.; Truhlar D. G. with assistance from Iron, J. M. A.; Martin, M. L. University of Minnesota, Minneapolis, MN, 2008.
(20) (a) Zhao, Y.; Truhlar, D. G. *Theor. Chem. Acc.* **2008**, *120*, 215. (b) Zhao, Y.; Truhlar, D. G. *Acc. Chem. Res.* **2008**, *41*, 157.
(21) Zhao, Y.; Truhlar, D. G. *J. Chem. Phys.* **2006**, *125*, 194101.
(22) Dunning, T. H., Jr. *J. Chem. Phys.* **1989**, *90*, 1007.
(23) Dolg, M. *Effective Core Potentials. In Modern Methods and Algorithms of Quantum Chemistry*; John von Neumann Institute for Computing: Jülich, 2000; Vol. 1, p 479.
(24) Martin, J. M. L.; Sundermann, A. *J. Chem. Phys.* **2001**, *114*, 3408.
(25) Peterson, K. A.; Figgen, D.; Goll, E.; Stoll, H.; Dolg, M. *J. Chem. Phys.* **2003**, *119*, 11113.
(26) (a) Dunlap, B. I. *J. Chem. Phys.* **1983**, *78*, 3140. (b) Dunlap, B. I. *THEOCHEM* **2000**, *529*, 37.
(27) Truhlar, D. G. "2006 Schrödinger Medal Lecture: New Density Functionals with Broad Applicability for Thermochemistry, Thermochemical Kinetics, Noncovalent Interactions, Transition Metals, and Spectroscopy" presented at the Eighth Triennial Congress of the World Association of Theoretical and Computational Chemistry (WATOC), Sydney, Australia, September 14−19, 2008.
(28) (a) Mennucci, B.; Tomasi, J. *J. Chem. Phys.* **1997**, *106*, 5151. (b) Cancès, E.; Mennucci, B.; Tomasi, J. *J. Chem. Phys.* **1997**, *107*, 3032. (c) Cossi, M.; Barone, V.; Mennucci, B.; Tomasi, J. *Chem. Phys. Lett.* **1998**, *286*, 253. (d) Cossi, M.; Scalmani, G.; Rega, N.; Barone, V. *J. Chem. Phys.* **2002**, *117*, 43. (e) Mennucci, B.; Cancès, E.; Tomasi, J. *J. Phys. Chem. B* **1997**, *101*, 10506. (f) Tomasi, J.; Mennucci, B.; Cancès, E. *THEOCHEM* **1999**, *464*, 211.
(29) Reed, A. E.; Curtiss, L. A.; Weinhold, F. *Chem. Rev.* **1988**, *88*, 899.
(30) Mulliken, R. S. *J. Chem. Phys.* **1955**, *23*, 1833.